



# $^{222}\text{Rn}$ and $\text{CO}_2$ monitoring in soil and indoor atmosphere to understand changes in the gaseous dynamics of Rull cave (Spain)

Concepción Pla<sup>1</sup> · María Candela Ruiz<sup>2</sup> · Sara Gil-Oncina<sup>2</sup> · Noé García-Martínez<sup>2</sup> · Juan Carlos Cañaveras<sup>2</sup> · Soledad Cuezva<sup>3</sup> · Ángel Fernández-Cortés<sup>4</sup> · Sergio Sánchez-Moral<sup>5</sup> · David Benavente<sup>2</sup>

Received: 7 October 2022 / Accepted: 6 April 2023  
© The Author(s) 2023

## Abstract

Rull cave is a karstic cave located in Vall d'Ebo (Alicante, Southeast of Spain) developed in massive Miocene conglomerates and Cretaceous limestones. Processes in soil above Rull cave and outdoor atmosphere directly influence the underground environment of the cave. Continuous and discrete monitoring of cave atmosphere and soil (from 2012 to 2022) allows to characterise the spatial distribution and temporal variations of the gaseous concentration ( $^{222}\text{Rn}$  and  $\text{CO}_2$ ) and understand the relationship between the processes which occurred in the 3-component system (soil-cave-atmosphere). Besides the presence of visitors, Rull cave maintains stable values of mean temperature (16.2 °C) and relative humidity (97.6%). In an annual cycle the cave presents two different gaseous stages (stagnation and ventilation). Maximum average values of  $\text{CO}_2$  and  $^{222}\text{Rn}$  concentration are reached within the stagnation stage, in the warmest period of the year. On the contrary, in the ventilation stage (in the coldest months) the cave reaches the lowest concentrations in its inner atmosphere. For the study period, daily average  $\text{CO}_2$  and  $^{222}\text{Rn}$  concentrations are 2008 ppm and 1745 Bq/m<sup>3</sup>, respectively. Results show that the dynamics of  $^{222}\text{Rn}$  and  $\text{CO}_2$  in the cave air follow different patterns defined by the complex relationships between external and internal factors. Findings from this study provide substantial information about the environmental situation of the cave atmosphere in terms of air quality for visitors and workers.

**Keywords** Advection · Gaseous diffusion · Microclimatic monitoring · Air quality

## Introduction

Concrete evidence shows that the vadose zone of karst terrains contains a large amount of gases, stored in cracks and voids in soil, bedrock or unconsolidated sediment (Benavente et al. 2010; Bourges et al. 2012; Fernandez-Cortés et al. 2015). Some research on the subject has studied

the presence of a wide variety of major, minor, and trace gases such as  $\text{CO}_2$ ,  $\text{O}_2$ ,  $^{222}\text{Rn}$ ,  $\text{CH}_4$ , among others, which are naturally produced, transported and stored within the underground karstic networks (Gregorič et al. 2013; Guillon et al. 2016; Matthey et al. 2021; Rowberry et al. 2016).

Underground caves are one of the principal components of the karst systems (Lonoy et al. 2020; Nyssen et al. 2020). They develop from the empty spaces in bedrock to configure differentiated environments with conditions that make them suitable natural laboratories for gas and microenvironmental monitoring (García-Anton et al. 2014; Lacanette et al. 2013; Sauro et al. 2019).

Cave atmospheres are often enriched in those gases found within the voids and cracks of the porous network. In caves with certain degrees of isolation, indoor concentrations are much higher than normal atmospheric values. For instance,  $\text{CO}_2$  or  $^{222}\text{Rn}$  concentrations of several thousand ppmv and Bq/m<sup>3</sup>, respectively, have been recorded inside studied caves (Álvarez-Gallego et al. 2015; Martín-Pozas et al. 2022a, b; Matthey et al. 2021; Pla et al. 2020). The abundance of these

✉ Concepción Pla  
c.pla@ua.es

<sup>1</sup> Department of Civil Engineering, University of Alicante, Alicante, Spain  
<sup>2</sup> Department of Earth and Environmental Sciences, University of Alicante, Alicante, Spain  
<sup>3</sup> Department of Geology, Geography and Environment Science, University of Alcalá, Madrid, Spain  
<sup>4</sup> Department of Biology and Geology, University of Almería, Almería, Spain  
<sup>5</sup> Department of Geology, National Museum of Natural Sciences (MNCN-CSIC), Madrid, Spain

gases is a consequence of a variety of sources. CO<sub>2</sub> in caves is mainly produced by microbial decay of organic matter and roots respiration in external soil and then transported to the cave atmosphere by diffusion; it is degassed from seepages or water streams, or exhaled by cave visitors as they breathe (Baldini et al. 2006; Benavente et al. 2015; Kuzyakov 2006; Peyraube et al. 2018). Depending on the geological context, CO<sub>2</sub> can also have an endogenous origin, as in hypogenic karst systems. Combining both scenarios and considering that karstification occurs in carbonate outcrops all across the globe (Ford and Williams 2007), large volumes of CO<sub>2</sub> produced and stored in underground environments are underestimated as contributors to the global carbon cycle (Fernandez-Cortes et al. 2015; Martin-Pozas et al. 2022a; Pla et al. 2016a; Serrano-Ortiz et al. 2010).

As CO<sub>2</sub>, radon is accumulated in underground caves, although both gases have different origin. Radon is a radioactive noble gas that exists naturally in the form of three isotopes: <sup>222</sup>Rn, <sup>220</sup>Rn and <sup>219</sup>Rn. The most stable and environmentally relevant one, <sup>222</sup>Rn, is formed by alpha decay of <sup>226</sup>Ra, and ultimately from <sup>238</sup>U; it has a half-life of 3.82 days. On the other hand, <sup>220</sup>Rn comes from the <sup>232</sup>Th disintegration and it has a short-lived isotope with a half-life of 55.60 s. <sup>219</sup>Rn is a member of the <sup>235</sup>U chain and decays most rapidly, having a half-life of about 3.92 s. Thus, in underground cave studies, <sup>220</sup>Rn and <sup>219</sup>Rn can be a practically negligible component to the total measured radon (Cinelli et al. 2019).

Releases of radon from soils and rocks to the atmosphere take place through the following processes (Moed et al. 1988): (1) emanation; radon atoms formed from the decay of <sup>226</sup>Ra escape from the grains into the interstitial space between them. It depends on the size particle (texture), <sup>226</sup>Ra content, and temperature and water content (emanation coefficient increases as temperature and water content). (2) Transport by diffusion and advective flow; it causes the movement of the emanated radon atoms through the soil profile to the ground surface. <sup>222</sup>Rn transport decreases as soil moisture increases because soil water reduces porosity and cross pore section, blocking gas movement in soils. (3) Exhalation; from radon atoms that have been transported to the ground surface and then exhaled to the atmosphere.

At present, underground environments (caves, basements, mines, etc.) capture the attention of researchers due to the human exposure to potentially hazardous substances in confined places where gases may accumulate and may become a health risk (Gil-Oncina et al. 2022; Smetanova et al. 2020; Smith et al. 2019; Weng et al. 2021), e.g. CO<sub>2</sub> or <sup>222</sup>Rn in high concentrations.

In this line, the EH40/2005 (2011) establishes for CO<sub>2</sub> a long-term exposure limit (8 h) of 5000 ppm at the workplace. For indoor radon concentrations in workplaces, the EU Member States established national reference levels for

the annual average activity concentration in the air that shall not be higher than 300 Bq/m<sup>3</sup>, following the Council Directive 2013/59/EURATOM (2014) of 5 December 2013, laying down basic safety standards for protection against the dangers arising from exposure to ionizing radiation. Above this radon level, studies are necessary to evaluate the exposure of workers to the environmental radiation, as well as the adoption of control measures aiming to reduce this exposure. Nowadays, especially for guides and maintenance staff of show caves, this subject is under consideration by studying the possible scenarios of exposition. The studies aim to prevent health risks as consequence of overexposure to high CO<sub>2</sub> concentrations (Smith 1999) and radon levels over the recommended yearly averaged levels by laws (Álvarez-Gallego et al. 2015; Sainz et al. 2018, 2020).

Thus, the study of cave atmospheres constitutes a key factor for both assessing the cave air quality and understanding the cave dynamics. The latter often shows seasonal variations in gaseous concentrations (CO<sub>2</sub> and <sup>222</sup>Rn) because of the relationship between outdoor and cave temperatures, as well as the behaviour of other important factors such as rainfall, barometric pressure, relative humidity, soil water content and temperature, among others (Cao et al. 2021; Cuezva et al. 2011; Pla et al. 2016a; Prelovšek et al. 2018). To understand the relationships between the different variables that influence cave dynamics it is essential to conduct a proper monitoring of the cave microenvironment, and the soil and atmosphere above it. For this purpose, a wide range of techniques has been applied to investigate the evolution of the gaseous concentrations in caves and its links with environmental parameters. For instance, complex analyses have been performed in confined environments and these, coupled with different tools such as statistics, entropy of curves, decomposition methods, wavelet analysis, global modelling technique, etc., have provided conclusive results (Denis and Cremoux 2002; Fernandez-Cortes et al. 2011; Galiana-Merino et al. 2014; Mihailović et al. 2015; Peyraube et al. 2018; Pla et al. 2016b, 2020; Sáez et al. 2021).

Variations in soil parameters have a direct influence on cave conditions. Studies about soil evolution above caves are not abundant (Garcia-Anton et al. 2017, 2014; Pla et al. 2017) although they are necessary for a better understanding of cave conditions, since the migration of gases from soil into caves (especially CO<sub>2</sub>, but also <sup>222</sup>Rn) has been defined as one of the main responsible of gaseous concentration in caves.

The aim of this study is to evaluate the evolution of gas concentration within the soil above Rull cave to understand changes in the cave gaseous dynamics, since previous studies revealed that they are closely related (Pla et al. 2016a, 2017, 2020). This study comprises discrete regular sampling complemented with continuous environmental monitoring in both soil and cave, with a focus on <sup>222</sup>Rn and CO<sub>2</sub>. The

evolution of these gases will be analysed to assess the relationships between soil and cave interior. Conclusions will help to preserve the quality of the cave atmosphere and evaluate possible risks related to the potentially hazardous substances that might be present within the cave.

## Materials and methods

### Study site

The study site is located in Rull cave (38° 48' 40" N, 0° 10' 38" W, Vall d'Ebo, Alicante), in Southeast Spain. Nearly 10 years of data sets (2012–2022) were produced from the continuous measurements of environmental variables and gaseous concentrations within the cave and the soil above it.

Above the cave, the silty-silty loam soil profile has a thickness below 1 m and presents a fine to coarse texture with no differentiated horizons. Soil is mainly composed of clay minerals and fine quartz, calcite and feldspars grains. Rull cave is developed in both massive Miocene conglomerates with considerable textural and petrophysical complexity, which were deposited on Cretaceous limestones (Pla et al. 2016a, 2017). These conglomerates conform the host rock of the cave, which has a thickness varying from 9 to 23 m. Conglomerates are composed of limeclasts, calcite cement, and matrix, which has a calcitic composition with a minor amount of iron oxides, quartz grains and clay minerals.

Inside the cave, calcite speleothems such as stalactites, columns, flowstones and draperies are common, and fallen blocks of different sizes are present due to old ceiling collapses (or breakdown) (Pla et al. 2014). Cave sediments came from weathering detritus (the insoluble component of the bedrock, left behind when the bedrock is dissolved) and soil washdown (sediments that migrate into the cave from the land surface above it). Cave sediments are distributed throughout the cave floor, which contain calcite, quartz, clay minerals, and feldspars. The uranium and thorium composition (obtained from ICP-MS; ALS Limited) present different values according to their mineralogical composition and clay content. The uranium concentrations for the soil, host-rock, cave sediments, and speleothems are, respectively, 3.14, 0.37, 2.23 and 0.09 ppm, whereas thorium concentrations are, respectively, 14.35, 0.09, 10.4 and <0.05 ppm.

The cave is a roughly rounded single room with an exposed surface of 1535 m<sup>2</sup> and holding 9915 m<sup>3</sup> inside, with the entrance located in the highest sector. The height inside the room is variable, with a maximum of 20 m (Fig. 1). Multiple C3 plants, Mediterranean vegetation and microorganisms grow in this soil profile (Pla et al. 2016a, b, 2017). The site has a Csa climate type, according to a slightly modified Köppen–Geiger Classification (AEMET-IM 2011),

which consists of warm annual temperatures with a dry and hot summer.

At the cave location and for the studied period (November 2012–July 2022), the environmental variables considered were temperature, relative humidity and pressure, with daily average values of 16.1 °C, 69.9% and 963.1 mbar, respectively. The average annual precipitation (2013–2021) is 553 mm. In the cave interior, temperature, relative humidity and pressure are, respectively, 16.2 °C, 97.6% and 963.3 mbar. Daily average CO<sub>2</sub> and <sup>222</sup>Rn concentrations are 2008 ppm and 1745 Bq/m<sup>3</sup>, respectively. In addition, the cave annually receives, on average, 15,000 visitors although the number changes over the year affected by seasonality. Easter period and summer months present the highest affluence of people.

From February 2015 to July 2022 the conditions of the outside soil above the cave were also recorded. In this period the daily average soil temperature and volumetric water content were 16.3 °C and 0.21 m<sup>3</sup>/m<sup>3</sup>, respectively.

### Environmental measurements

Environmental measurements in Rull Cave were performed with different weather stations and environmental probes, which changed within the study period (Pla et al. 2016a, 2017). Currently there is one datalogger HOBO H22-001 (Onset Computer, USA) recording synchronous and continuous microclimatic measurements inside the cave. It is connected to the electrical supply, and it has a security battery to ensure autonomy in case of power failure. The probes connected to the datalogger provide hourly temperature and relative humidity (HMP45AC, Vaisala, Finland; accuracies of ±0.2 °C and ±2.0%, respectively), CO<sub>2</sub> concentration (GMP252, Vaisala, Finland; accuracy of ±40 ppm and measurement range of 0–10,000 ppm) and barometric pressure (S-BPB-CM50 Sensor, Onset Computer, USA; accuracy of ±3.0 mbar). In addition, a Radim 5WP radon monitor (SSM&SISIE, Prague; accuracy of ±12 Bq/m<sup>3</sup>) measures <sup>222</sup>Rn concentration, also with hourly periodicity.

Atmospheric conditions outside the cave are continuously measured using a H21 Hobo Weather Station (Onset Computer, USA) coupled with an S-THB-M002 temperature and relative humidity sensor (Onset Computer, USA; accuracies of ±0.21 °C and ±2.5%, respectively), an S-BPB-CM50 barometric pressure sensor (Onset Computer, USA; accuracy of ±3.0 mbar) and an S-RGF-M002 Davis rain gauge sensor (Onset Computer, USA; accuracy of ±4%).

Hourly measurements of soil conditions (temperature and volumetric water content) are performed with a HOBO U12 logger (Onset, USA; accuracy of ±0.5 °C) and an ECHO EC-5 probe (Decagon Devices, USA; accuracy of ±1–2%) connected to an Em5b logger (Decagon Devices, USA). These probes are located at 10 cm depth in the soil cave.

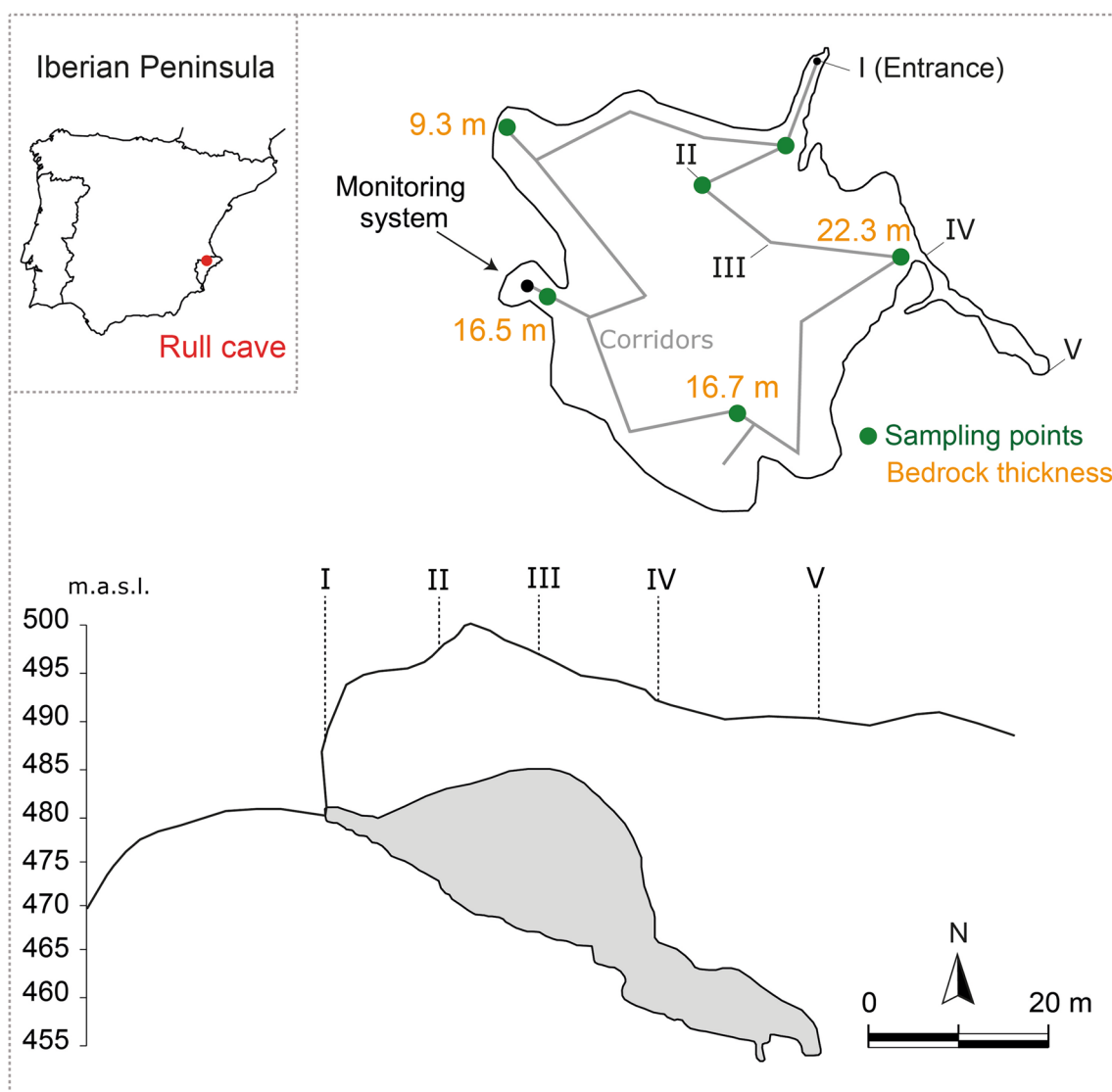


**Fig. 1** Location and cave map. Adapted from Nadal et al. (1990). Sampling points of discrete measurements are indicated in green colour. Measured bedrock thickness is also indicated. Points indicated by

the roman numbers in the top figure (plan view) correspond to the same locations in the bottom figure (vertical profile)

For the 10-year period under analysis, some data are missing due to instrument failure or temporary power cuts affecting some probes. In the case of the  $\text{CO}_2$  and  $^{222}\text{Rn}$  time series, the seasonal variations of both tracer gases are coeval, so the data gaps for  $\text{CO}_2$  could be easily inferred from the time evolution of radon levels.

### Gas sampling and analysis

Since January 2014, discrete sampling of air from the outside atmosphere, soil air and cave atmosphere are performed to characterise the spatial distribution and temporal variation of  $\text{CO}_2$  concentration and its  $\delta^{13}\text{C}$  signature. The sampling period varies through the study period. In the sampling

procedure, air is pumped and saved into 1 L Tedlar gas sampling bags, and then analysed using a Picarro G2101-i analyser (California, USA; accuracy of  $\pm 0.3\%$  for  $\delta^{13}\text{C}$  after 5 min of analysis) which uses cavity ring-down spectroscopy (CRDS-WS) (Crosson 2008).

Three in-house standards with certified gas mixtures and known  $\text{CO}_2$  concentration (7000 ppm, 400 ppm, and zero- $\text{CO}_2$ ), supplied by Abello Linde-Spain, were used at the beginning and the end of each analytical session by CRDS to calibrate the  $\text{CO}_2$  concentration values from the air samples. The proper functioning of the CRDS analyser and its performance specifications regarding  $\delta^{13}\text{C}$ - $\text{CO}_2$  analyses were periodically checked and calibrated relative to two reference standards (USGS40 with  $\delta^{13}\text{C}$  VPDB =  $-26.4\%$  and

USGS41a with  $\delta^{13}\text{C VPDB} = +37.6\text{‰}$ , supplied by USGS/Reston Stable Isotope Laboratory), whose carbon isotopic signal was regularly determined by a combustion module (Costech, USA) coupled to the CRDS analyser (CM-CRDS system). The consecutive rounds of  $\delta^{13}\text{C-CO}_2$  analyses of air samples were calibrated against the  $\text{CO}_2$  obtained by CM-CRDS system for the following internal secondary standards:  $\text{NaHCO}_3$  ( $\delta^{13}\text{C VPDB} = -10.9\text{‰}$ ), sugarcane ( $\delta^{13}\text{C VPDB} = -11.7\text{‰}$ ), acetanilide ( $\delta^{13}\text{C VPDB} = -26.3\text{‰}$ ) and urea ( $\delta^{13}\text{C VPDB} = -49.2\text{‰}$ ).

Since September 2021, discrete sampling of  $^{222}\text{Rn}$  concentration in soil gas and cave air is also monthly conducted. The gas inside the 2 L Tedlar sampling bags, collected in the cave and from the soil, is measured using AlphaGUARD DF2000 (Saphymo GmbH, Frankfurt am Main, Germany) which has a pulse ionization chamber (alpha spectroscopy) that allows measurement in diffusion and flow operation modes. For this study, the air samples were analysed using the 1-min flow mode, with a 0.3 L/min pump flow, over a 15-min period. A loop was employed for the analysis to measure the gas contained in different sampling bags collected in identical locations.

Radon exhalation,  $E$  ( $\text{Bq}/(\text{m}^2\text{s})$ ), was estimated in an accumulation chamber of PMMA (polymethyl methacrylate), with 20 cm inner diameter. The chamber was located over a single PVC collar, which was permanently installed in the soil. The accumulation phase initially describes a linear growth with time,  $t$  (s), of the radon concentration in the accumulation chamber [ $^{222}\text{Rn}$ ] ( $\text{Bq}/\text{m}^3$ ). Radon exhalation ( $E$ ) is calculated as (Eq. 1):

$$E = (V/S) \cdot ([^{222}\text{Rn}]/t). \quad (1)$$

where  $V$  ( $\text{m}^3$ ) is the effective accumulation chamber volume and  $S$  ( $\text{m}^2$ ) is the exhaling soil surface within the accumulation chamber. The  $^{222}\text{Rn}$  concentration was recorded using an AlphaE (Saphymo GmbH, Frankfurt am Main, Germany) for 4 h.

Since September 2021, inside the cave, the  $\text{CO}_2$  and  $^{222}\text{Rn}$  discrete sampling was carried out while simultaneously measuring air temperature at each sampling point with a Vaisala HM70 portable probe (Vaisala, Finland; accuracy of  $\pm 0.2$  °C).

## Results and discussion

### Annual variations in Rull cave atmosphere

For the 10-year period under analysis (Fig. 2), Rull cave exhibits an annual gaseous cycle with two differentiated states. This pattern has also been found in many studies of gas dynamics within caves (Cao et al. 2021; Liñán et al.

2008; Wong and Banner 2010). In summer, with exterior temperatures ( $T_{\text{out}}$ ) being higher than temperature inside the cave ( $T_{\text{in}}$ ) (Fig. 2d), the cave atmosphere remains stagnated. This period is characterised by an increased accumulation of both gases  $\text{CO}_2$  and  $^{222}\text{Rn}$ , reaching the maximum concentrations registered for the annual cycle. On the contrary, during the colder period of the year, the cave enters a ventilation stage with the air renewal causing a remarkable depletion of the gaseous concentrations (Fig. 2a, b). These seasonal variations in  $\text{CO}_2$  and  $^{222}\text{Rn}$  concentrations are mainly a consequence of the relationships between external and cave temperatures (Pla et al. 2016a; Fig. 2a, b, d). The time series resulting of continuous measurements in Rull cave indicates that the average daily values of  $\text{CO}_2$  and  $^{222}\text{Rn}$  concentrations vary from a minimum of 478 ppm and 404  $\text{Bq}/\text{m}^3$ , respectively (October to March/April), to a maximum of 3966 ppm and 4185  $\text{Bq}/\text{m}^3$  (April/May to September). Although the cave receives visitors almost every day (Fig. 2b),  $\text{CO}_2$  variations due to these visits are not substantial, and baseline concentrations are recovered after a short time period which varies, normally, from 1 to 72 h (Pla et al. 2016b, 2020). Seasonal variations of external temperature changed throughout the annual cycles and, consequently, the duration of each seasonal pattern of thermal gradient between the cave and the outer atmosphere ( $T_{\text{in}} > T_{\text{out}}$  or, on the contrary,  $T_{\text{in}} < T_{\text{out}}$ ) varies from year to year. This fact implies that the beginning and end of each stage defined by the tracer gases concentrations and their variations (ventilation and stagnation) present inter-annual variations, although the amplitude of the seasonal variations of both tracer gases are similar over the years (Fig. 2a, b, d). This triggers the cave gaseous recharge or discharge, which is nevertheless also influenced by other environmental variables such as rainfall, soil temperature or soil water content (Fig. 2c) (Pla et al. 2016a, 2020). Atmospheric pressure and pressure inside the cave are nearly coincident, which points to the permanent barometric equilibrium between both environments (Fig. 2d).

Continuous measurements of temperature ( $T_{\text{in}}$ ) inside Rull cave confirm that its atmosphere presents high environmental stability, with annual variations of  $\pm 1.4$  °C (Fig. 2d). For the 10-year studied period the maximum measured temperature is 16.8 °C (during winter), while the lowest was 15.4 °C (during summer). In addition, discrete measurements of cave temperature (turned into average values) performed from September 2021 to August 2022 (Fig. 3), indicate that the sector closest to the entrance is the warmest, especially the westernmost sector in which the overlying bedrock has the smallest thickness (Figs. 1, 3). The southernmost sector, farthest from the cave entrance, presents the lowest temperatures.

Spatial distribution of  $\text{CO}_2$  and  $^{222}\text{Rn}$  (average values of the discrete sampling; September 2021–August 2022)

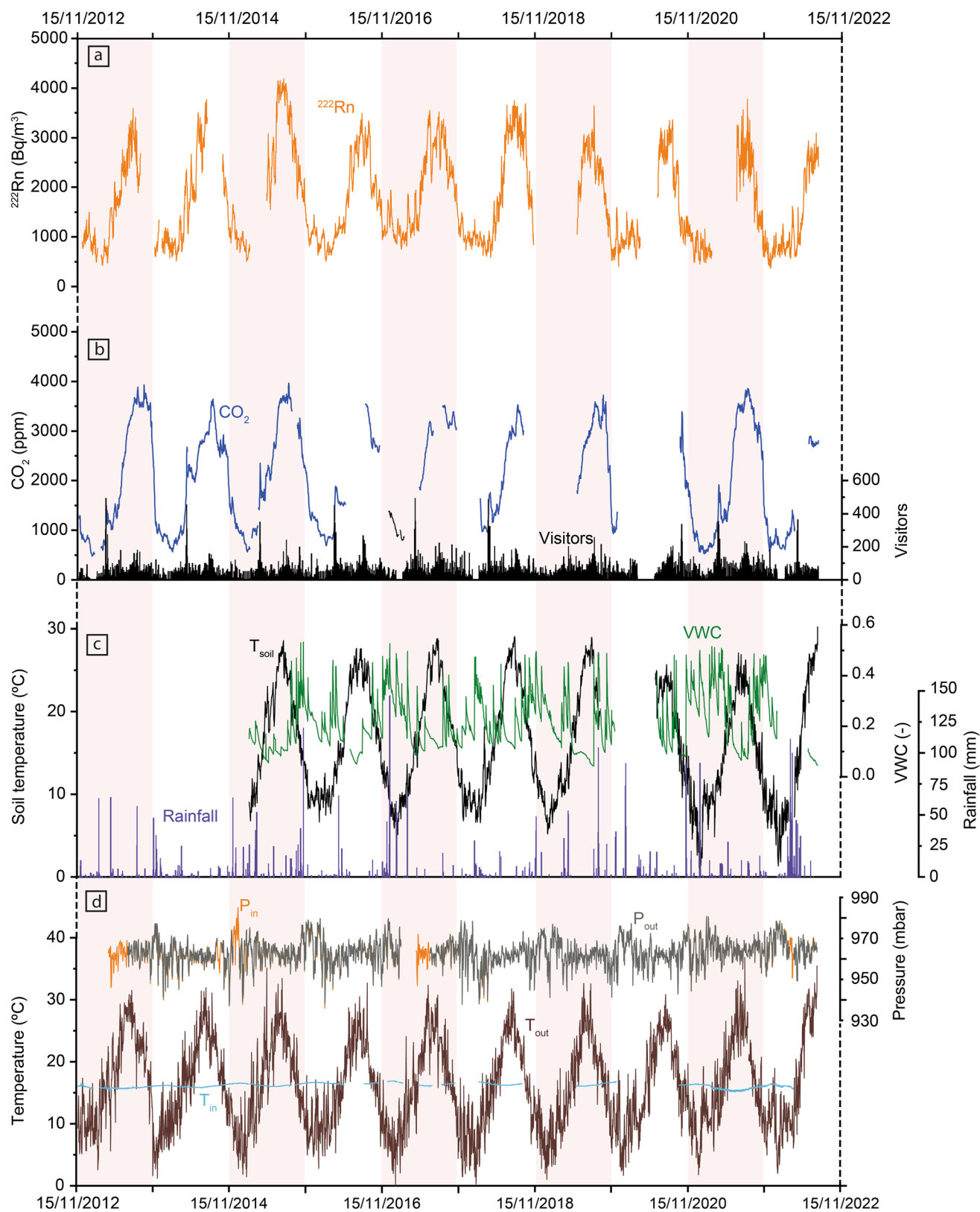


**Fig. 2** Environmental conditions in the cave, the outdoor atmosphere and soil for the study period. **a**  $^{222}\text{Rn}$  concentration ( $\text{Bq}/\text{m}^3$ ), **b**  $\text{CO}_2$  (ppm) and visitors. **c** Soil conditions: soil temperature ( $^{\circ}\text{C}$ ) and

volumetric water content (VWC,  $\text{m}^3/\text{m}^3$ ), and rainfall (mm). **d** Outdoor and indoor temperatures ( $^{\circ}\text{C}$ ) and barometric pressures (mbar). Shaded vertical areas mark the 1-year division period

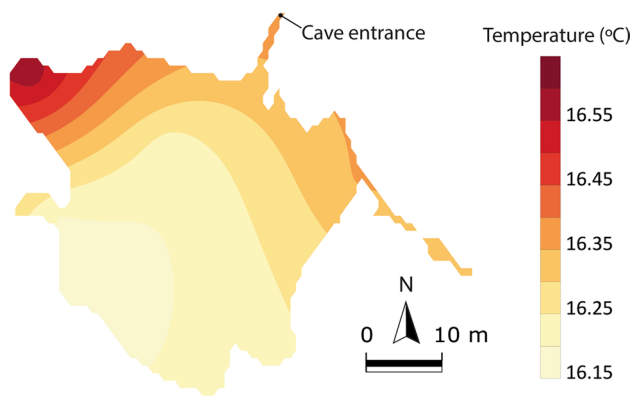


**Fig. 3** Spatial distribution of mean annual air temperature in Rull cave (°C). Measurements (average values) performed in the discrete sampling (2021–2022 period)

reveals that in the two stages of the cave (stagnation and ventilation), the lowest concentrations of both gases are found near the entrance (Fig. 4) highlighting that this area presents the higher rate of air exchange with the exterior. The spatial distribution of both gases follows a similar pattern directly related to the morphology and the cave air circulation. Results obtained from the discrete sampling are coincident with the continuous measurements of gas concentration, pointing to a predominant air renewal in the coldest months when the concentration reaches the minimum values. During the stagnation period, the maximum values of  $\text{CO}_2$  and  $^{222}\text{Rn}$  concentration in the cave atmosphere confirm that in the warmest months the air exchange rate with the external atmosphere is at the minimum.

### $\text{CO}_2$ in soil and its relationship with cave $\text{CO}_2$

Previous studies confirm that the Rull cave gaseous dynamics is governed by diffusive and advective fluxes responsible for the final gas concentrations in the cave atmosphere (Pla et al. 2016a, 2017). Both processes can exist simultaneously, and the prevalence of one over the other during a certain period is caused by the relationship between the different environmental variables in atmosphere, soil, and cave. When the cave temperature ( $T_{\text{in}}$ ) is higher than the outdoor temperature ( $T_{\text{out}}$ ) in the coldest months of the year, an advective gaseous flux between the exterior and interior air masses is predominant because of the density difference. On the contrary, when the relationship between temperatures is inverted, the ventilation due to the density gradient becomes non-existent and the colder and thus denser air within the cave remains nearly stagnant. During this stage, the gaseous diffusion from soil towards the cave contributes (depending on soil and cave conditions) to the increase in  $\text{CO}_2$ , reaching higher concentrations that last until the exterior temperature decreases below the cave temperature.

Maximum  $\text{CO}_2$  concentration in the cave is a consequence of the  $\text{CO}_2$  soil production (Amundson et al. 1998; Faimon et al. 2012; Garcia-Anton et al. 2017) and its diffusion rates (Jabro et al. 2012; Jassal et al. 2004; Wang et al. 2019). Therefore, although  $\text{CO}_2$  ranges from 3500 to 3900 ppm during summer, the precise annual maximum value is defined every year by soil respiration and a prevailing gaseous transport in the soil-rock porous system (Pla et al. 2016a). The incoming flux of soil-derived  $\text{CO}_2$  to the cave atmosphere is noticed by the decrease of the isotopic signature  $\delta^{13}\text{C}\text{-CO}_2$  as  $\text{CO}_2$  of cave air rises.

The sampling of soil  $\text{CO}_2$  above Rull cave has been carried out since 2014 (Fig. 5). Soil  $\text{CO}_2$  also presents annual variations, although they are less recognizable than the cycles inside the cave, probably because of the discrete measurements not being performed with a regular time interval between them. Measurements in April–May–June and September–October usually present the highest values of soil  $\text{CO}_2$  concentrations (Fig. 5) although this varies between cycles. The maximum  $\text{CO}_2$  concentrations in soil, occurred during spring, are a consequence of the soil production under moderate soil temperatures and are influenced by the soil water content, thus related to rainfall. For instance, the rainfall occurred between March and May in 2022 (778 mm) was extraordinarily abundant when compared to the rest of the studied time series (the average annual precipitation is 553 mm for the period 2013–2021) and coincident with the maximum measured soil  $\text{CO}_2$  concentration (4866 ppm) in May 2022. High soil  $\text{CO}_2$  concentrations measured in autumn (October 2014: 2622 ppm; October 2017: 2714 ppm; September 2019: 4841 ppm) are also related to moderate soil temperatures and enough water within the soil due to rainfall. Maximum soil  $\text{CO}_2$  values registered in spring normally coincide with lower  $\text{CO}_2$  cave concentrations (Fig. 5) and maximum soil  $\text{CO}_2$  values registered in autumn normally coincide with decreasing  $\text{CO}_2$  cave concentrations.

Relationships between soil-cave-atmosphere are highlighted with the results of the air sampling and the analyses of the  $\text{CO}_2$  abundance and its carbon isotopic signature. Within the soil, carbon dioxide is mainly derived from the respiration of living plants and the decomposition of organic matter by soil microorganisms (Amundson et al. 1998).  $\text{CO}_2$  derived from C3 plant roots and microbial respiration in soils with organic matter content is characterised by values of  $\delta^{13}\text{C}\text{-CO}_2$  ranging from  $-25.0$  to  $-27.5\%$  VDP (Amundson et al. 1998; Cerling et al. 1991; Di Martino et al. 2016, 2020; Kuzyakov 2006). Consequently  $\delta^{13}\text{C}\text{-CO}_2$  evolution in soil and inside Rull cave emphasises the periods of major soil  $\text{CO}_2$  production (lowest values of  $\delta^{13}\text{C}\text{-CO}_2$  in soil being coincident with maximum soil  $\text{CO}_2$  concentration). The soil-produced  $\text{CO}_2$  can diffuse into the cave atmosphere under certain conditions of soil porous network. Heavy isotopes diffuse more

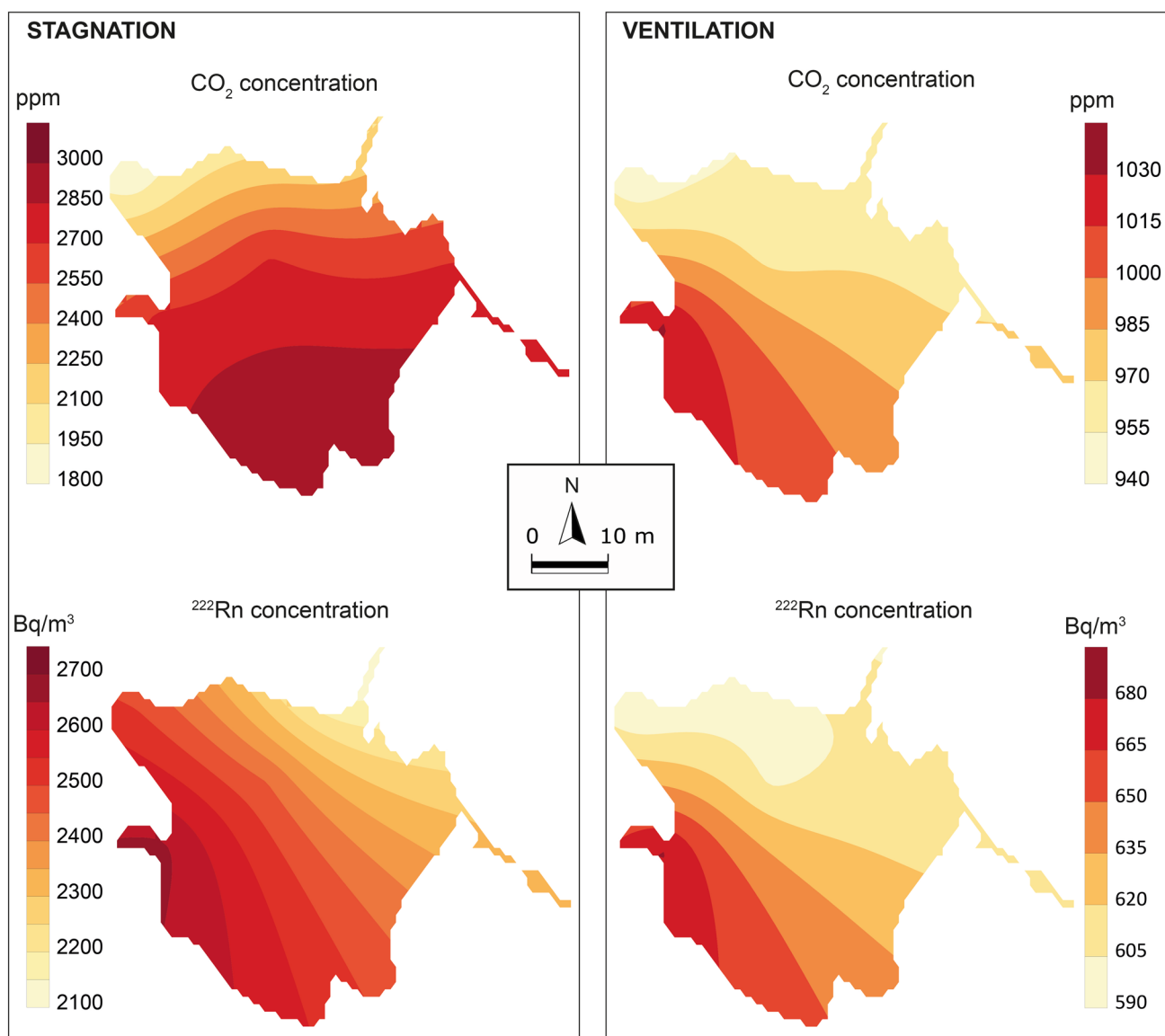


**Fig. 4** Spatial distribution of mean annual concentrations of  $\text{CO}_2$  (ppm) and  $^{222}\text{Rn}$  ( $\text{Bq/m}^3$ ). Concentration corresponds to the average values of the discrete sampling measurements developed from September 2021 to August 2022. The concentrations for the stagnation

stage are calculated from samples collected in the period May–September while concentrations for the ventilation stage are calculated from samples collected in the period October–April

slowly, leading to an enrichment of  $^{12}\text{C}$  (lighter  $\delta^{13}\text{C}\text{-CO}_2$  values) of the soil-derived  $\text{CO}_2$ . A maximum theoretical kinetic fractionation of 4.4‰ has been reported for the diffusion processes through the soil (Capasso et al. 2001). This transport requires a certain time, but when this diffused soil  $\text{CO}_2$  enters the cave, it causes a likely  $^{13}\text{C}$  depletion of  $\text{CO}_2$  reaching the lowest values (lightest). There is a delay between maximums in soil and cave because of the gaseous transport through soil and rock.

When soil  $\text{CO}_2$  mixes with the cave gaseous atmosphere it is diluted with the external air (enriched in  $\delta^{13}\text{C}\text{-CO}_2$ ) that enters to Rull cave by advective mechanisms predominant

from October to April–May (Fig. 5) and which is responsible for the lowest  $\text{CO}_2$  concentrations in the cave atmosphere.

The Keeling-plot approach (Keeling 1958) is based on a simplified two-end member model where the concentration and isotopic ratio of the cave-air  $\text{CO}_2$  result from the proportional mixing of the background atmosphere and a second source (soil-derived) with an isotopically light  $\text{CO}_2$ -rich component. Two results can be obtained from the Keeling plot: (1) the intercept value of the lineal Keeling function in the  $\delta^{13}\text{C}\text{-CO}_2$  axis corresponds to the theoretical isotopic signal of the soil-derived  $\text{CO}_2$  source, and (2) the relative contribution of  $\text{CO}_2$  from the outer atmosphere that

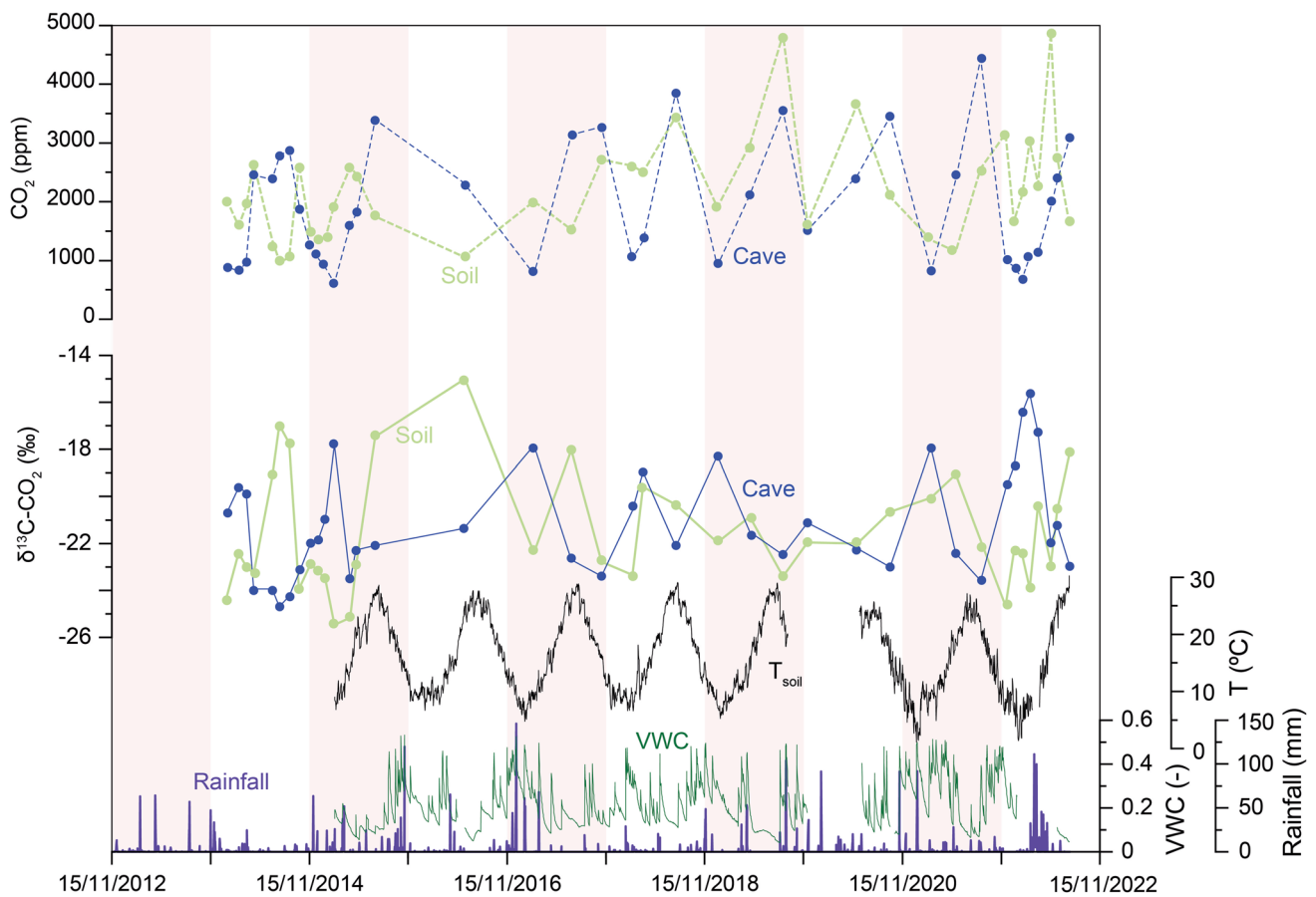


**Fig. 5** Soil and cave  $\text{CO}_2$  concentration and  $\delta^{13}\text{C-CO}_2$  (‰) (discrete measurements). Continuous time series of soil above Rull cave (soil temperature and volumetric water content) and rainfall. Shaded vertical areas mark the 1-year division period

is present in the cave air, in function of the proximity of the data pairs of cave air to each end member. The Keeling plot for the atmosphere-soil-cave system demonstrates that the  $\text{CO}_2$  concentration in Rull cave air is the result of mixing the background atmospheric  $\text{CO}_2$  with the soil-produced one. This diagram highlights the prevalence of the soil organic  $\text{CO}_2$  component in the cave atmosphere. The linear fitting of the data, obtained from the discrete samplings, intercepts the y-axis ranging from  $-24.80$  to  $-26.55\text{‰}$  (Fig. 6), which is in the range defining the characteristic values for  $\delta^{13}\text{C-CO}_2$  derived from  $\text{C}_3$  plant roots and microbial respiration (Amundson et al. 1998; Cerling et al. 1991; Kuzyakov 2006).

The y-axis interception value for both stages confirms that  $\text{CO}_2$  within the cave primarily comes from roots and microbial respiration in the soil above the cave. The most  $\delta^{13}\text{C}$ -depleted air  $\text{CO}_2$  during the ventilation stage highlights the predominance of the soil  $\text{CO}_2$  origin also when rates of dilution are predominant in the cave atmosphere. In the periods with higher external temperatures and scarce rainfall, the porous network of soil keeps open and connected to the external atmosphere. As a consequence, the direct

connection between soil and cave is neglected because soil produced  $\text{CO}_2$  migrates to the external atmosphere. On the contrary, with moderate temperatures and water content in soil (on average, nearly  $15\text{ °C}$  and  $0.17$ ), diffusion from soil to cave is active and coincident with ventilation (early spring). This triggers that in the ventilation stage (Fig. 6a) the y-intercept value is more negative (closer to the soil  $\delta^{13}\text{C-CO}_2$  value) than in the stagnation period. During the ventilation stage, the porous network of soil is partially filled with water and a  $\text{CO}_2$  influx from soil to cave atmosphere prevails in comparison with gas fluxes from soil to the open atmosphere. This provokes an input of  $^{12}\text{C}$ -depleted gas (soil-derived  $\text{CO}_2$ ) to the cave at atmosphere and, consequently, the y-intercept value of the Keeling plot becomes more negative during this stage.

### $^{222}\text{Rn}$ in soil and its relationship with cave $^{222}\text{Rn}$

Although  $^{222}\text{Rn}$  production mechanism is different from  $\text{CO}_2$ , the  $^{222}\text{Rn}$  concentration within the cave describes the same annual cycles than  $\text{CO}_2$  (Fig. 2) and follows a similar spatial distribution (Fig. 4). The spatial distribution of

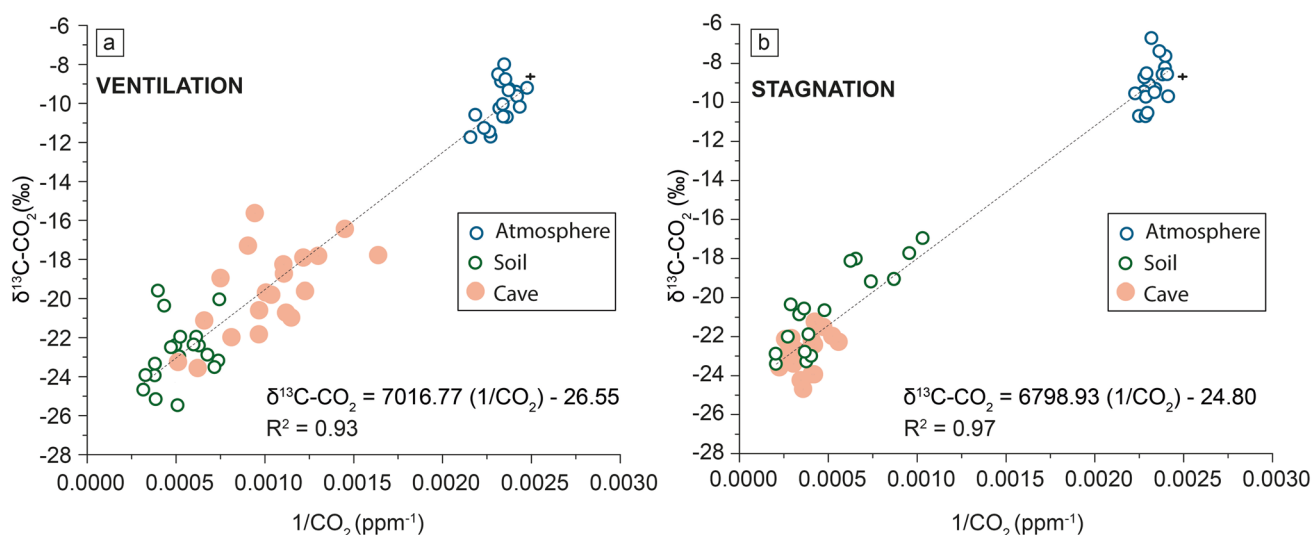


**Fig. 6** Keeling plot for the discrete sampling in Rull soil, exterior air and cave air. Keeling plot is represented for the two predominant stages: ventilation (**a**) and recharge (**b**). The cross marks indicate the range of  $\text{CO}_2$  and  $\delta^{13}\text{C-CO}_2$  of the background atmosphere at exterior during the monitoring period (2012–2022) obtained from the Centro de Investigación de la Baja Atmósfera (CIBA), Spain, which belongs

to the Global Monitoring Laboratory of the National Oceanic and Atmospheric Administration (NOAA) (<https://gml.noaa.gov/dv/site/index.php?stacode=CIB>; last access: 19/12/2022). These data ranges are representative of atmospheric  $\text{CO}_2$  for latitudes of the Iberian Peninsula and, therefore, comparable with the local atmosphere of the study area

gases in the cave is dependent of the air density gradient between the cave and the outer atmosphere and controls the seasonal variations of both tracer gases. These processes affect the entire air masses, without distinguishing between single gases. In addition, the diffusion coefficients in the air of  $\text{CO}_2$  and  $^{222}\text{Rn}$  are similar. For instance, at 25 °C, they are  $0.15 \cdot 10^{-4} \text{ m}^2/\text{s}$  and  $0.12 \cdot 10^{-4} \text{ m}^2/\text{s}$  for  $\text{CO}_2$  and  $^{222}\text{Rn}$ , respectively (Lerman 1979; Nazaroff 1992). Thus, maximum concentrations of both gases are reached simultaneously, confirming the annual dependency of gas concentrations on the temperature gradient, and thus on the predominance of gaseous diffusion or advection.

Production and exhalation of  $^{222}\text{Rn}$  depend primarily on the host rock, speleothems and sediments of the cave, and also on the soil above it.  $^{222}\text{Rn}$  derives from radium decay and its emanation rate and transport through the porous networks are dependent on the different environmental and geological conditions (Álvarez-Gallego et al. 2015; Lario et al. 2005).

$^{222}\text{Rn}$  produced in soil and host rock migrates within the rock mass (Ferry et al. 2002) by diffusion and/or advection through pores, macro-pores, and fractures (Ajayi et al. 2018; Ferry et al. 2002; Nazaroff and Nero 1988), reaching the cave indoors. Transport of  $^{222}\text{Rn}$  and  $\text{CO}_2$  dissolved in water increases when soil is saturated. Under this situation, water permeability becomes critical in the gas transport. Both gases are soluble in water and present similar solubility: at 25 °C, the fraction solubility of  $\text{CO}_2$  and  $^{222}\text{Rn}$  is  $6.15 \cdot 10^{-4}$  and  $1.67 \cdot 10^{-4}$ , respectively (Crovetto 1991; IUPAC

1979) and diffusion coefficient in water is  $1.95 \cdot 10^{-9} \text{ m}^2/\text{s}$  and  $1.37 \cdot 10^{-9} \text{ m}^2/\text{s}$  for  $\text{CO}_2$  and  $^{222}\text{Rn}$ , respectively (Lerman 1979; Nazaroff 1992). Thus, waters with dissolved  $^{222}\text{Rn}$  and  $\text{CO}_2$  can flow through pores and fractures of the host-rock and enter the cave, where the degasification of dripping waters can contribute to increase the gaseous concentration.

The  $^{222}\text{Rn}$  measured in Rull soil emanates into the atmosphere with a particular rate, inherent to the soil composition and nature of the samples (Amin 2015; Amin et al. 2008). Exhalation in Rull soil might be related to a particular characteristic rate but the variations from 0.05 to 0.005  $\text{Bq}/\text{m}^2\text{s}$  (Fig. 7) are a consequence of the environmental variables and soil conditions. The soil water content affects soil  $^{222}\text{Rn}$  concentration mainly through its influence on the radon emanation coefficient in soil (Benavente et al. 2019; Sun et al. 2004). Water content in the soil promotes  $^{222}\text{Rn}$  exhalation up to a certain level of this water content and retains the  $^{222}\text{Rn}$  afterwards (Yang et al. 2019). Thus, maximum values of  $^{222}\text{Rn}$  concentration in the soil during spring followed by a temporal delay of maximum exhalation rates in Rull soil may be mainly related to the variations in soil water content due to rainfalls. Previous studies in different field sites (Kojima and Nagano 2005; Megumi and Mamuro 1973; Schery et al. 1984) confirmed that the radon exhalation rate did not change significantly with light rainfall (13 mm), but it decreased dramatically with heavy rainfall (93 mm) and remained low for several days after heavy rainfall.

$^{222}\text{Rn}$  produced in soil depends on uranium and thorium concentration, size particle (texture), and temperature and

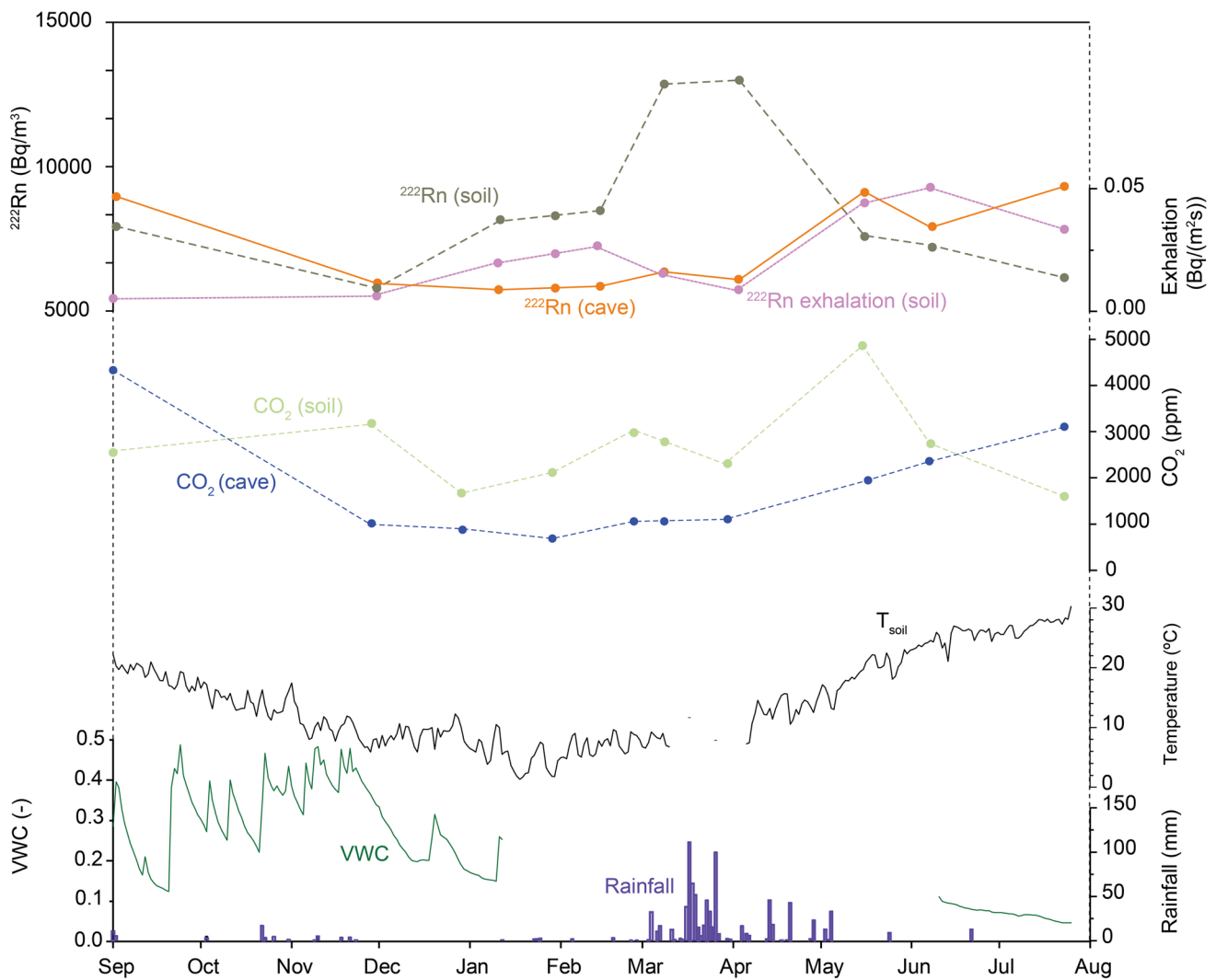


**Fig. 7** Soil and cave  $^{222}\text{Rn}$  and  $\text{CO}_2$  concentrations and  $^{222}\text{Rn}$  exhalation rates (discrete measurements). Continuous time series of soil above Rull cave (soil temperature and volumetric water content) and rainfall

water content, which affect the emanation coefficient and it is a consequence of rainfall and water condensation (Fig. 7). Although the time series of  $^{222}\text{Rn}$  soil measurements is shorter compared to the  $\text{CO}_2$  soil measurements,  $^{222}\text{Rn}$  concentration in soil (discrete measurements) increases significantly when rainfall occurs. A pattern similar to the one described by soil  $\text{CO}_2$  is repeated by soil  $^{222}\text{Rn}$ . The rainfall occurred between March and May in 2022 is coincident with the maximum measured  $^{222}\text{Rn}$  concentration in soil. Maximum values of  $^{222}\text{Rn}$  are reached before maximum  $\text{CO}_2$ , but this delay might be related to the different origin of each gas. In Rull site, the  $^{222}\text{Rn}$  emitted by the soil is also transported by diffusion into the cave. The consequence of this process is a rising in  $^{222}\text{Rn}$  in the cave atmosphere, which strengthens in absence of ventilation.

The uranium and thorium concentration in the materials of the soil-cave system depends on their mineralogical

composition and specifically on clay content. As described previously, soil above the cave and cave sediment present a higher uranium and thorium concentration. Moreover, both soil and cave sediments are powder materials, and the emanation is enhanced in comparison to host-rock and speleothems, although their volume in the cave is higher than soil and cave sediments.

Part of the  $^{222}\text{Rn}$  produced by soil migrates into the cave by diffusion since soil  $^{222}\text{Rn}$  concentration is higher than in the cave (Fig. 7) as occurs with  $\text{CO}_2$ .  $^{222}\text{Rn}$  transport from soil behaves similarly to  $\text{CO}_2$ . However, due to the radioactive nature of  $^{222}\text{Rn}$ , its concentration shall decrease over time once the diffusion became negligible. In this situation, the emanation of  $^{222}\text{Rn}$  from cave sediments, host-rock and speleothems, which might be constant through the year (due to the microenvironmental conditions of the cave), contributes to increase  $^{222}\text{Rn}$  cave concentration. Furthermore, the

$^{222}\text{Rn}$  concentration in the cave is also dependent on the previously described ventilation mechanisms governing the cave dynamics (Fig. 2), which will be responsible of the lowest gaseous concentration.

In addition, although it has not been quantified for this study, dripping water degassing might also contribute to increasing  $^{222}\text{Rn}$  concentration in caves.  $^{222}\text{Rn}$  in dripping water is also related to precipitation that percolates through the soil-cave profile and depends on its residence time within the profile (Nakasone et al. 2021). Previous studies in other caves have highlighted that, at certain gaseous stages, dripping water degassing was responsible for the increases in  $^{222}\text{Rn}$  concentration of cave atmosphere (Tang et al. 2020). However, in Rull cave dripping waters are not abundant (Pla et al. 2020) and thus the contribution of  $\text{CO}_2$  or  $^{222}\text{Rn}$  degassing from seepage waters to increase cave gaseous concentration might be low.

### Exposure to $\text{CO}_2$ and $^{222}\text{Rn}$ in Rull cave

Time series recorded in Rull cave are useful to estimate adequate and healthy exposition to the gaseous atmosphere, considering the cave workers and visitors (the site receives an annual average of 15,000 visitors). In Rull cave, for the study period (November 2012–July 2022), maximum values obtained from daily average concentrations of  $\text{CO}_2$  and  $^{222}\text{Rn}$  were 3966 ppm and 4185 Bq/m<sup>3</sup>, respectively. The EH40/2005 (2011) establishes for  $\text{CO}_2$  a long-term exposure limit (8 h) of 5000 ppm at the workplace. Thus, workers and visitors' exposition to  $\text{CO}_2$  is considered safe since they never exceed this limit.

In addition, for  $^{222}\text{Rn}$ , ICRP (2017) recommends, for the specific situations of indoor work involving exposures in tourist caves, a dose coefficient of 6 mSv per mJ h/m<sup>3</sup> which is equivalent, approximately, to 20 mSv per WLM (ICRP 2017). Complementary, national legislation (RD 783/2001 2001; CSN, Instrucción IS-33 2012) establishes that workers receiving radiation due to their work activity higher than 6 mSv/year must undergo strict physical examinations. Consequently, it would be recommended, particularly, for the Rull cave workers not to surpass this threshold.

Between 2013 and 2014, the total time that guides spent inside the cave was monitored daily. Data from these years could be adopted as representative of the ordinary annual cycle since conditions have not changed significantly since then. Afterwards, average monthly individual times were obtained considering (1) that there are 3 permanent guides alternating visits inside the cave and (2) the variability in the number of visits (as time inside the cave) within a year (Fig. 2b). Attending to this, Table 1 shows the calculated effective dose received in a regular year by an individual guide.

The calculated dose is 5.97 mSv/year which is near to the recommended maximum exposure (6 mSv/year) for which national legislation indicates special control measures for workers. With an accurately planification of the visits, particularly when the cave is in the stagnation stage, workers could be less exposed to radiation. Microclimatic monitoring of Rull cave assists in the determination of potentially hazardous concentrations, to comply with the official air quality standards.

**Table 1** Total dose per month (mSv) calculated for an individual guide in Rull cave

Month	Average time spent inside the cave for individual guide (h)	Accumulated time (h)	$^{222}\text{Rn}$ concentration (average monthly values for 2013–2014) (Bq/m <sup>3</sup> )	Dose (mSv) (dose conversion factor, DCF=20 mSv/WLM)	Accumulated dose (mSv)
January	13.00	13.00	927	0.15	0.15
February	13.00	26.00	858	0.14	0.29
March	21.00	47.00	890	0.23	0.53
April	16.00	63.00	1235	0.25	0.77
May	21.00	84.00	1711	0.45	1.23
June	19.00	103.00	2537	0.61	1.83
July	28.00	131.00	2988	1.05	2.88
August	40.00	171.00	3023	1.52	4.40
September	23.00	194.00	2500	0.72	5.12
October	22.00	216.00	1768	0.49	5.61
November	16.00	232.00	1094	0.22	5.83
December	11.00	243.00	980	0.14	5.97

Data of the average time spent inside the cave and the correspondent  $^{222}\text{Rn}$  concentration are monthly average values for 2013 and 2014

## Conclusions

Rull cave gas dynamics is the result of complex relationships between soil, cave and external atmosphere. This study demonstrates that environmental parameters are responsible for the CO<sub>2</sub> and <sup>222</sup>Rn concentrations and variations in soil and cave air.

Rull cave gas dynamics (CO<sub>2</sub> and <sup>222</sup>Rn concentration) follows an annual pattern with a stagnation period and a ventilation period, although CO<sub>2</sub> and <sup>222</sup>Rn origins are different. These periods are a consequence of the thermal relationships between interior and outdoor atmospheres, that cause advective ventilation through the host rock fractures. The spatial distribution of both gases in the cave also follows a pattern directly related to the morphology and the cave air circulation. The lowest concentrations of both gases are found near the entrance, where the cave presents a higher rate of air exchange with the exterior.

The analyses of CO<sub>2</sub> abundance and the isotopic signature δ<sup>13</sup>C-CO<sub>2</sub> in the soil-cave-atmosphere system demonstrate that the CO<sub>2</sub> concentration in Rull cave air is the result of mixing the background atmospheric CO<sub>2</sub> with the soil-produced one. The soil organic CO<sub>2</sub> component, originated from soil organic respiration, is prevalent within the cave environment. Maximum soil CO<sub>2</sub> concentrations occurring during spring are a consequence of the soil production under moderate soil temperatures and are influenced by the soil water content and thus related to the rainfall occurrence.

<sup>222</sup>Rn concentration in soil rises significantly after rainfall since the radon emanation increases along with soil water content. The <sup>222</sup>Rn, produced by soil, migrates towards the cave by diffusion through the host rock. Still, the clayed sediments of the cave are the major contributors to <sup>222</sup>Rn concentration in the cave atmosphere. In the cave, dripping water sites are scarce and have low drip rates, so the dissolved <sup>222</sup>Rn in water might represent a minor contribution to the cave air radon concentration. The <sup>222</sup>Rn derived from the different materials inside Rull cave would be nearly constant for the whole year, but it is affected by the ventilation mechanisms governing the cave dynamics.

The continuous monitoring of Rull cave provides substantial information about the environmental situation of the cave atmosphere in terms of air quality for visitors and workers. The maximum average concentrations of CO<sub>2</sub> and <sup>222</sup>Rn in Rull cave and exposition times and doses comply with the recommendations of the legislation. However, in case of <sup>222</sup>Rn, the calculated doses received for workers are close to the maximums recommended by the official standards. Consequently, an accurately planification of the visits (particularly in the months when the cave atmosphere presents maximum concentrations), is necessary for them to be less exposed to radiation.

**Acknowledgements** This work was supported by the Spanish Ministry of Science, Innovation and Universities (project RTI2018-099052-BI00), and Regional Government of Comunidad Valenciana (Spain) (project AICO/2020/175), and with collaboration of the project PID2019-110603RB-I00. A pre-doctoral research fellowship (PRE2019-088294) was awarded to S.G.O. (linked to the project RTI2018-099052-BI00). A pre-doctoral research fellowship (GRI-SOLIAP/2020/124) was awarded to M.C.R. by the Department of Innovation, Universities, Science and Digital Society of the Generalitat Valenciana, and a pre-doctoral research fellowship (FPU20/05157) was awarded to N.G.M. by the Spanish Ministry of Science, Innovation and Universities.

**Author contributions** Conceptualization: CP, DB; methodology: CP, MCR, SG-O; NG-M, AF-C, DB. Formal analysis and investigation: CP, MCR, SG-O; NG-M, AF-C, DB; writing—original draft preparation: CP, DB, MCR; writing—review and editing: SG-O, NG-M, AF-C, JCC, SC, AF-C, SS-M; funding acquisition: DB.

**Funding** Open Access funding provided thanks to the CRUE-CSIC agreement with Springer Nature.

**Data availability** Data generated or analysed during this study are included in this article, and the datasets used or analysed during the current study are available from the corresponding author on reasonable request.

## Declarations

**Conflict of interest** The authors declare no competing interests.

**Open Access** This article is licensed under a Creative Commons Attribution 4.0 International License, which permits use, sharing, adaptation, distribution and reproduction in any medium or format, as long as you give appropriate credit to the original author(s) and the source, provide a link to the Creative Commons licence, and indicate if changes were made. The images or other third party material in this article are included in the article's Creative Commons licence, unless indicated otherwise in a credit line to the material. If material is not included in the article's Creative Commons licence and your intended use is not permitted by statutory regulation or exceeds the permitted use, you will need to obtain permission directly from the copyright holder. To view a copy of this licence, visit <http://creativecommons.org/licenses/by/4.0/>.

## References

- AEMET-IM (2011) Iberian Climate Atlas. Agencia Estatal de Meteorología (Spain) and Departamento de Meteorología e Clima, Instituto de Meteorología (Portugal), Madrid
- Ajayi KM, Shahbazi K, Tukkaraja P, Katzenstein K (2018) A discrete model for prediction of radon flux from fractured rocks. *J Rock Mech Geotech Eng* 10:879–892. <https://doi.org/10.1016/j.jrmge.2018.02.009>
- Álvarez-Gallego M, Cuezva S, Fernández-Cortés A, García-Antón E, Sánchez Moral S (2015) High radon levels in subterranean environments: monitoring and technical criteria to ensure human safety (case of Castañar cave, Spain). *J Environ Radioact* 29:19–29. <https://doi.org/10.1016/j.jenvrad.2015.03.024>
- Amin RM (2015) A study of radon emitted from building materials using solid state nuclear track detectors. *J Radiat Res Appl Sci* 8:516–522. <https://doi.org/10.1016/j.jrras.2015.06.001>

- Amin RM, Mansy M, Eissa MF, Eissa HM, Shahin FM (2008) Assessment of natural radioactivity and radon exhalation rate in Sannur cave, eastern desert of Egypt. *J Radiol Prot* 28:213–222. <https://doi.org/10.1088/0952-4746/28/2/005>
- Amundson R, Stern L, Baisden T, Wang Y (1998) The isotopic composition of soil and soil-respired CO<sub>2</sub>. *Geoderma* 82:83–114. [https://doi.org/10.1016/S0016-7061\(97\)00098-0](https://doi.org/10.1016/S0016-7061(97)00098-0)
- Baldini JLU, Baldini LM, McDermott F, Clipson N (2006) Carbon dioxide sources, sinks, and spatial variability in shallow temperate zone caves: evidence from Ballynamintra Cave, Ireland. *J Cave Karst Stud* 68:4–11
- Benavente J, Vadillo I, Carrasco F, Soler A, Liñán C, Moral F (2010) Air carbon dioxide contents in the vadose zone of a Mediterranean Karst. *Vadose Zone J* 9:126–136. <https://doi.org/10.2136/vzj2009.0027>
- Benavente J, Vadillo I, Liñán C, del Rosal Y, Carrasco F (2015) Influence of the ventilation of a karst show cave on the surrounding vadose CO<sub>2</sub> reservoir (Nerja, South Spain). *Environ Earth Sci* 74:7731–7740. <https://doi.org/10.1007/s12665-015-4709-8>
- Benavente D, Valdés-Abellán J, Pla C, Sanz-Rubio E (2019) Estimation of soil gas permeability for assessing radon risk using Rosetta pedotransfer function based on soil texture and water content. *J Environ Radioact* 208–209:105992. <https://doi.org/10.1016/j.jenvrad.2019.105992>
- Bourges F, Genthon P, Genty D, Mangin A, D'Hulst D (2012) Comment on “Carbon uptake by karsts in the Houzhai Basin, southwest China” by Junhua Yan et al. *J Geophys Res.* <https://doi.org/10.1029/2012JG001937>
- Cao M, Lei JQ, He QF, Zeng Z, Lu XF, Jiang YJ (2021) Rainfall-driven and hydrologically-controlled variations in cave CO<sub>2</sub> sources and dynamics: evidence from monitoring soil CO<sub>2</sub>, stream flow and cave CO<sub>2</sub>. *J Hydrol.* <https://doi.org/10.1016/j.jhydrol.2021.126060>
- Capasso G, D'Alessandro W, Favara R, Inguaggiato S, Parello F (2001) Kinetic isotope fractionation of CO<sub>2</sub> carbon due to diffusion processes through the soil. In: 10th international symposium on water–rock interaction, Villasimius, Italy. pp 1497–1499
- Cerling TE, Solomon DK, Quade J, Bowman JR (1991) On the isotopic composition of carbon in soil carbon dioxide. *Geochim Cosmochim Acta* 55:3403–3405. [https://doi.org/10.1016/0016-7037\(91\)90498-T](https://doi.org/10.1016/0016-7037(91)90498-T)
- Cinelli G, Tollefsen T, Bossew P, Gruber V, Bogucarskis K, De Felice L, De Cort M (2019) Digital version of the European Atlas of natural radiation. *J Environ Radioact* 196:240–252. <https://doi.org/10.1016/j.jenvrad.2018.02.008>
- Crosson ER (2008) A cavity ring-down analyzer for measuring atmospheric levels of methane, carbon dioxide, and water vapor. *Appl Phys B Lasers O* 92:403–408. <https://doi.org/10.1007/s00340-008-3135-y>
- Crovetto R (1991) Evaluation of solubility data of the system CO<sub>2</sub>–H<sub>2</sub>O from 273 K to the critical point of water. *J Phys Chem Ref Data* 20:575–589. <https://doi.org/10.1063/1.555905>
- CSN, Instrucción IS-33 (2012) Instrucción IS-33, de 21 de diciembre de 2011, del Consejo de Seguridad Nuclear, sobre criterios radiológicos para la protección frente a la exposición a la radiación natural
- Cuezva S, Fernandez-Cortes A, Benavente D, Serrano-Ortiz R, Kowalski AS, Sanchez-Moral S (2011) Short-term CO<sub>2</sub>(g) exchange between a shallow karstic cavity and the external atmosphere during summer: role of the surface soil layer. *Atmos Environ* 45:1418–1427. <https://doi.org/10.1016/j.atmosenv.2010.12.023>
- Denis A, Cremoux F (2002) Using the entropy of curves to segment a time or spatial series. *Math Geol* 34:899–914. <https://doi.org/10.1023/a:1021302922108>
- Di Martino RMR, Capasso G, Camarda M (2016) Spatial domain analysis of carbon dioxide from soils on Vulcano Island: Implications for CO<sub>2</sub> output evaluation. *Chem Geol* 444:59–70. <https://doi.org/10.1016/j.chemgeo.2016.09.037>
- Di Martino RMR, Capasso G, Camarda M, De Gregorio S, Prano V (2020) Deep CO<sub>2</sub> release revealed by stable isotope and diffuse degassing surveys at Vulcano (Aeolian Islands) in 2015–2018. *J Volcanol Geotherm Res* 401:106972. <https://doi.org/10.1016/j.jvolgeores.2020.106972>
- EH40/2005 Workplace Exposure Limits (2011) List of approved workplace exposure limits. Health and safety executive. Health and Safety Executive (HSE), Norwich, pp 9–26
- European Council Directive (2014) 2013/59/Euratom on basic safety standards for protection against the dangers arising from exposure to ionising radiation and repealing Directives 89/618/Euratom, 90/641/Euratom, 96/29/Euratom, 97/43/Euratom and 2003/122/Euratom. *Off J Eur J* L13(57):1–73
- Faimon J, Ličbinská M, Zajíček P (2012) Relationship between carbon dioxide in Balcarka cave and adjacent soils in the Moravian Karst region of the Czech Republic. *Int J Speleol.* <https://doi.org/10.5038/1827-806X.41.1.3>
- Fernandez-Cortes A, Sanchez-Moral S, Cuezva S, Benavente D, Abella R (2011) Characterization of trace gases' fluctuations on a 'low energy' cave (Castañar de Ibor, Spain) using techniques of entropy of curves. *Int J Climatol* 31:17. <https://doi.org/10.1002/joc.2057>
- Fernandez-Cortes A, Cuezva S, Garcia-Anton E, Alvarez-Gallego M, Pla C, Benavente D, Cañaveras JC, Calaforra JM, Matthey DP, Sanchez-Moral S (2015) Changes in the storage and sink of carbon dioxide in subsurface atmospheres controlled by climate-driven processes: the case of the Ojo Guareña karst system. *Environ Earth Sci* 74:7715–7730. <https://doi.org/10.1007/s12665-015-4710-2>
- Ferry C, Richon P, Beneito A, Cabrera J, Sabroux JC (2002) An experimental method for measuring the radon-222 emanation factor in rocks. *Radiat Meas* 35:579–583. [https://doi.org/10.1016/S1350-4487\(02\)00092-6](https://doi.org/10.1016/S1350-4487(02)00092-6)
- Ford D, Williams PD (2007) Karst hydrogeology and geomorphology. Wiley, Hoboken
- Galiana-Merino JJ, Pla C, Fernandez-Cortes A, Cuezva S, Ortiz J, Benavente D (2014) Environmental Wavelet Tool: continuous and discrete wavelet analysis and filtering for environmental time series. *Comput Phys Commun* 185:2758–2770. <https://doi.org/10.1016/j.cpc.2014.06.011>
- García-Anton E, Cuezva S, Fernandez-Cortes A, Benavente D, Sanchez-Moral S (2014) Main drivers of diffusive and advective processes of CO<sub>2</sub>-gas exchange between a shallow vadose zone and the atmosphere. *Int J Greenh Gas Control* 21:113–129. <https://doi.org/10.1016/j.ijggc.2013.12.006>
- García-Anton E, Cuezva S, Fernandez-Cortes A, Alvarez-Gallego M, Pla C, Benavente D, Cañaveras JC, Sanchez-Moral S (2017) Abiotic and seasonal control of soil-produced CO<sub>2</sub> efflux in karstic ecosystems located in Oceanic and Mediterranean climates. *Atmos Environ* 164:31–49. <https://doi.org/10.1016/j.atmosenv.2017.05.036>
- Gil-Oncina S, Valdes-Abellan J, Pla C, Benavente D (2022) Estimation of the Radon risk under different european climates and soil textures. *Front Public Health* 10:794557. <https://doi.org/10.3389/fpubh.2022.794557>
- Gregorič A, Vaupotič J, Gabrovšek F (2013) Reasons for large fluctuation of radon and CO<sub>2</sub> levels in a dead-end passage of a karst cave (Postojna Cave, Slovenia). *Nat Hazards Earth Syst Sci* 13:287–297. <https://doi.org/10.5194/nhess-13-287-2013>
- Guillon S, Gréau C, Pili E (2016) Continuous monitoring of the vadose zone gas phase by mass spectrometry. *Vadose Zone J* 15(vzj2015):0168. <https://doi.org/10.2136/vzj2015.12.0168>
- ICRP (2017) Occupational intakes of radionuclides—part 3. ICRP Publication 137. *Ann ICRP* 46(3/4)

- IUPAC (1979) Solubility data series, volume 2: krypton, xenon, and radon—gas solubilities. Pergamon, Amsterdam
- Jabro JD, Sainju UM, Stevens WB, Evans RG (2012) Estimation of CO<sub>2</sub> diffusion coefficient at 0–10 cm depth in undisturbed and tilled soils. *Arch Agron Soil Sci* 58:1–9. <https://doi.org/10.1080/03650340.2010.506482>
- Jassal RS, Black TA, Drewitt GB, Novak MD, Gaumont-Guay D, Nescic Z (2004) A model of the production and transport of CO<sub>2</sub> in soil: predicting soil CO<sub>2</sub> concentrations and CO<sub>2</sub> efflux from a forest floor. *Agric for Meteorol* 124:219–236. <https://doi.org/10.1016/j.agrformet.2004.01.013>
- Keeling CD (1958) The concentration and isotopic abundances of atmospheric carbon dioxide in rural areas. *Geochim Cosmochim Acta* 13:322–334. [https://doi.org/10.1016/0016-7037\(58\)90033-4](https://doi.org/10.1016/0016-7037(58)90033-4)
- Kojima H, Nagano K (2005) Simulation of radon exhalation at Kanto Loam with very low permeability. *J Atmos Electr* 25:1–9. <https://doi.org/10.1541/jae.25.1>
- Kuzyakov Y (2006) Sources of CO<sub>2</sub> efflux from soil and review of partitioning methods. *Soil Biol Biochem* 38:425–448. <https://doi.org/10.1016/j.soilbio.2005.08.020>
- Lacanette D, Large D, Ferrier C, Aujoulat N, Bastian F, Denis A, Jurado V, Kervazo B, Konik S, Lastennet R, Malaurent P, Saiz-Jimenez C (2013) A laboratory cave for the study of wall degradation in rock art caves: an implementation in the Vézère area. *J Archaeol Sci* 40:894–903. <https://doi.org/10.1016/j.jas.2012.10.012>
- Lario J, Sanchez-Moral S, Cañaveras J, Cuezva S, Soler V (2005) Radon continuous monitoring in Altamira Cave (northern Spain) to assess user's annual effective dose. *J Environ Radioact* 80:161–174. <https://doi.org/10.1016/j.jenvrad.2004.06.007>
- Lerman A (1979) *Geochemical processes: water and sediment environments*. Wiley, New York
- Liñán C, Vadillo I, Francisco C (2008) Carbon dioxide concentration in air within the Nerja Cave (Malaga, Andalusia, Spain). *Int J Speleol* 37:99–106. <https://doi.org/10.5038/1827-806X.37.2.2>
- Lonoy B, Tveranger J, Pennos C, Whitaker F, Lauritzen SE (2020) Geocellular rendering of cave surveys in paleokarst reservoir models. *Mar Pet Geol*. <https://doi.org/10.1016/j.marpetgeo.2020.104652>
- Martin-Pozas T, Cuezva S, Fernandez-Cortes A, Cañaveras JC, Benavente D, Jurado V, Saiz-Jimenez C, Janssens I, Seijas N, Sanchez-Moral S (2022a) Role of subterranean microbiota in the carbon cycle and greenhouse gas dynamics. *Sci Total Environ* 831:154921. <https://doi.org/10.1016/j.scitotenv.2022.154921>
- Martin-Pozas T, Novakova A, Jurado V, Fernandez-Cortes A, Cuezva S, Saiz-Jimenez C, Sanchez-Moral S (2022b) Diversity of micro-fungi in a high radon cave ecosystem. *Front Microbiol*. <https://doi.org/10.3389/fmicb.2022.869661>
- Mattay DP, Atkinson TC, Hoffmann DL, Boyd M, Ainsworth M, Durell R, Latin JP (2021) External controls on CO<sub>2</sub> in Gibraltar cave air and ground air: implications for interpretation of delta C-13 in speleothems. *Sci Total Environ*. <https://doi.org/10.1016/j.scitotenv.2021.146096>
- Megumi K, Mamuro T (1973) Radon and thoron exhalation from the ground. *J Geophys Res* 78:1804–1808. <https://doi.org/10.1029/JB078i011p01804>
- Mihailović DT, Krmar M, Mimić G, Nikolić-Dorić E, Smetanová I, Holý K, Zelinka J, Omelka J (2015) A complexity analysis of <sup>222</sup>Rn concentration variation: a case study for Domica cave, Slovakia for the period June 2010–June 2011. *Radiat Phys Chem* 106:88–94. <https://doi.org/10.1016/j.radphyschem.2014.06.016>
- Moed BA, Nazaroff WW, Sextro RG (1988) Soil as a source of indoor radon: generation, migration and entry, radon and its decay products in indoor air. In: Nazaroff W, Nero A (eds) *Radon and its decay products in indoor air*. Wiley, New York, pp 57–112
- Nadal G, Vicens M, Pérez D (1990) Cova del Rull (Vall d'Ebo), 017 (Ali.-017-03VE-01C-03C). <https://cuevasalicante.espeleocv.org/es/>. Accessed Apr 2023
- Nakasone S, Ishimine A, Shiroma S, Masuda N, Nakamura K, Shiroma Y, Ooka S, Tanaka M, Kato A, Hosoda M, Akata N, Yasuoka Y, Furukawa M (2021) Temporal and spatial variation of radon concentrations in environmental water from Okinawa Island, South-western Part of Japan. *Int J Environ Res Public Health* 18:998. <https://doi.org/10.3390/ijerph18030998>
- Nazaroff WW (1992) Radon transport from soil to air. *Rev Geophys* 30:137–160. <https://doi.org/10.1029/92RG00055>
- Nazaroff WW, Nero AV (1988) *Radon and its decay products in indoor air*. Wiley, New York
- Nyssen J, Yonas M, Annys S, Ghebreyohannes T, Smidt W, Wel-eagerima K, Gebreselassie S, Sembroni A, Dramis F, Ek C, Causer D (2020) The Zeyi cave geosite in Northern Ethiopia. *Geoheritage*. <https://doi.org/10.1007/s12371-020-00446-7>
- Peyraube N, Lastennet R, Denis A, Malaurent P, Houillon N, Villanueva JD (2018) Determination and quantification of major climatic parameters influencing the CO<sub>2</sub> of Lascaux Cave. *Theor Appl Climatol* 133:1291–1301. <https://doi.org/10.1007/s00704-017-2255-x>
- Pla C, Muñoz-Cervera MC, Rodríguez-García MA, Cuevas-González J, Andreu JM, Garcíadel-Cura MA, Cuezva S, Cañaveras JC, Benavente D (2014) Espeleotemas en la Cueva del Rull (Vall d'Ebo, Alicante). 1er Congreso Iberoamericano y 5º Congreso Español sobre Cuevas Turísticas (CUEVATUR). Ayuntamiento de Aracena, Aracena (Spain). pp 333–341
- Pla C, Cuezva S, García-Anton E, Fernández-Cortés A, Cañaveras JC, Sánchez-Moral S, Benavente D (2016a) Changes in the CO<sub>2</sub> dynamics in near-surface cavities under a future warming scenario: factors and evidence from the field and experimental findings. *Sci Total Environ* 565:1151–1164. <https://doi.org/10.1016/j.scitotenv.2016.05.160>
- Pla C, Galiana-Merino JJ, Cuezva S, Fernández-Cortés A, Cañaveras JC, Benavente D (2016b) Assessment of CO<sub>2</sub> dynamics in subsurface atmospheres using the wavelet approach: from cavity—atmosphere exchange to anthropogenic impacts in Rull cave (Vall d'Ebo, Spain). *Environ Earth Sci* 75:446. <https://doi.org/10.1007/s12665-016-5325-y>
- Pla C, Cuezva S, Martínez-Martínez J, Fernández-Cortés A, García-Anton E, Fusi N, Crosta GB, Cuevas-González J, Cañaveras JC, Sánchez-Moral S, Benavente D (2017) Role of soil pore structure in water infiltration and CO<sub>2</sub> exchange between the atmosphere and underground air in the vadose zone: a combined laboratory and field approach. *CATENA* 149(Part 1):402–416. <https://doi.org/10.1016/j.catena.2016.10.018>
- Pla C, Fernández-Cortés A, Cuezva S, Galiana-Merino JJ, Cañaveras JC, Sánchez-Moral S, Benavente D (2020) Insights on climate-driven fluctuations of Cave <sup>222</sup>Rn and CO<sub>2</sub> concentrations using statistical and wavelet analyses. *Geofluids* 2020:8858295. <https://doi.org/10.1155/2020/8858295>
- Prelovšek M, Šebela S, Turk J (2018) Carbon dioxide in Postojna Cave (Slovenia): spatial distribution, seasonal dynamics and evaluation of plausible sources and sinks. *Environ Earth Sci* 77:289. <https://doi.org/10.1007/s12665-018-7459-6>
- RD 783/2001 (2001) Real Decreto 783/2001, de 6 de julio, por el que se aprueba el Reglamento sobre protección sanitaria contra radiaciones ionizantes
- Rowberry MD, Martí X, Frontera C, Van De Wiel MJ, Briestenský M (2016) Calculating flux to predict future cave radon concentrations. *J Environ Radioact* 157:16–26. <https://doi.org/10.1016/j.jenvrad.2016.02.023>
- Sáez M, Mangiarotti S, Cuezva S, Fernández-Cortés A, Molero B, Sánchez-Moral S, Benavente D (2021) Global models for <sup>222</sup>Rn and CO<sub>2</sub> concentrations in the cave of Altamira.

- Theor Appl Climatol 143:603–626. <https://doi.org/10.1007/s00704-020-03440-9>
- Sainz C, Rábago D, Celaya S, Fernández E, Quindós J, Quindós L, Fernández A, Fuente I, Arteche JL, Quindós LS (2018) Continuous monitoring of radon gas as a tool to understand air dynamics in the cave of Altamira (Cantabria, Spain). *Sci Total Environ* 624:416–423. <https://doi.org/10.1016/j.scitotenv.2017.12.146>
- Sainz C, Rábago D, Fernández E, Quindós J, Quindós L, Fernández A, Fuente I, Arteche JL, Quindós LS, Celaya S (2020) Variations in radon dosimetry under different assessment approaches in the Altamira Cave. *J Radiol Prot* 40:367. <https://doi.org/10.1088/1361-6498/ab6fd2>
- Sauro F, Pozzobon R, Santagata T, Tomasi I, Tonello M, Martínez-Frías J, Smets LMJ, Santana Gómez GD, Massironi M (2019) Volcanic caves of Lanzarote: a natural laboratory for understanding volcano-speleogenetic processes and planetary caves. In: Mateo E, Martínez-Frías J, Vegas J (eds) Lanzarote and Chinijo islands Geopark: from earth to space. Springer International Publishing, Cham, pp 125–142
- Schery SD, Gaeddert DH, Wilkening MJ (1984) Factors affecting exhalation of radon from a gravelly sandy loam. *J Geophys Res* 89:7299–7309. <https://doi.org/10.1029/JD089iD05p07299>
- Serrano-Ortiz P, Roland M, Sanchez-Moral S, Janssens IA, Domingo F, Goddérís Y, Kowalski AS (2010) Hidden, abiotic CO<sub>2</sub> flows and gaseous reservoirs in the terrestrial carbon cycle: review and perspectives. *Agric for Meteorol* 150:321–329. <https://doi.org/10.1016/j.agrformet.2010.01.002>
- Smetanova I, Holy K, Luhova L, Csicsay K, Haviarova D, Kunakova L (2020) Seasonal variation of radon and CO<sub>2</sub> in the Vazecka Cave, Slovakia. *Nukleonika* 65:153–157. <https://doi.org/10.2478/nuka-2020-0025>
- Smith GK (1999) Foul air in limestone caves and its effect on cavers. In: Federation CQAS (ed), 22nd Australian Speleological Federation's Conference Queensland (Australia). pp 44–58
- Smith ME, Dumitru OA, Burgehele BD, Cucos A, Onac BP (2019) Radon concentration in three Florida caves: Florida, Jennings, and Ocala. *Carbonates Evaporites* 34:433–439. <https://doi.org/10.1007/s13146-018-0473-7>
- Sun K, Guo Q, Cheng J (2004) The effect of some soil characteristics on soil radon concentration and radon exhalation from soil surface. *J Nucl Sci Technol* 41:1113–1117. <https://doi.org/10.1080/18811248.2004.9726337>
- Tang W, Lan G, Yang H, Yin J-J, Pu J (2020) Variations and influence factors of <sup>210</sup>Pb-specific radioactivity in modern calcite depositions in a subtropical cave, South China. *Appl Geochem* 113:104468. <https://doi.org/10.1016/j.apgeochem.2019.104468>
- Wang XL, Fu SL, Li JX, Zou XM, Zhang WX, Xia HP, Lin YB, Tian Q, Zhou LX (2019) Forest soil profile inversion and mixing change the vertical stratification of soil CO<sub>2</sub> concentration without altering soil surface CO<sub>2</sub> flux. *Forests*. <https://doi.org/10.3390/f10020192>
- Weng X, Luo WJ, Wang YW, Zeng GN, Wang SJ (2021) Spatiotemporal variations of radon concentration in the atmosphere of Zhijindong Cave (China). *Atmosphere*. <https://doi.org/10.3390/atmos12080967>
- Wong C, Banner JL (2010) Response of cave air CO<sub>2</sub> and drip water to brush clearing in central Texas: implications for recharge and soil CO<sub>2</sub> dynamics. *J Geophys Res* 115:G04018. <https://doi.org/10.1029/2010JG001301>
- Yang J, Busen H, Scherb H, Hürkamp K, Guo Q, Tschiersch J (2019) Modeling of radon exhalation from soil influenced by environmental parameters. *Sci Total Environ* 656:1304–1311. <https://doi.org/10.1016/j.scitotenv.2018.11.464>

**Publisher's Note** Springer Nature remains neutral with regard to jurisdictional claims in published maps and institutional affiliations.